SAR405838: An Optimized Inhibitor of MDM2–p53 Interaction That Induces Complete and Durable Tumor Regression

Shaomeng Wang[1,2,3,4], Wei Sun[1,2], Yujun Zhao[1,2], Donna McEachern[1,2], Isabelle Meaux[5], Cédric Barrière[5], Jeanne A. Stuckey[6], Jennifer L. Meagher[6], Longchuan Bai[1,2], Liu Liu[1,2], Cassandra Gianna Hoffman-Luca[1,3], Jianfeng Lu[1,2], Sanjeev Shangary[1,2], Shanghai Yu[1,2], Denzil Bernard[1,2], Angelo Aguilar[1,2], Odette Dos-Santos[5], Laurent Besret[5], Stéphane Guerif[5], Pascal Pannier[5], Dimitri Gorge-Bernat[5], and Laurent Debussche[5]

Abstract

Blocking the oncoprotein murine double minute 2 (MDM2)–p53 protein–protein interaction has long been considered to offer a broad cancer therapeutic strategy, despite the potential risks of selecting tumors harboring p53 mutations that escape MDM2 control. In this study, we report a novel small-molecule inhibitor of the MDM2–p53 interaction, SAR405838 (MI-77301), that has been advanced into phase I clinical trials. SAR405838 binds to MDM2 with $K_i = 0.88$ nmol/L and has high specificity over other proteins. A cocrystal structure of the SAR405838:MDM2 complex shows that, in addition to mimicking three key p53 amino acid residues, the inhibitor captures additional interactions not observed in the p53–MDM2 complex and induces refolding of the short, unstructured MDM2 N-terminal region to achieve its high affinity. SAR405838 effectively activates wild-type p53 *in vitro* and in xenograft tumor tissue of leukemia and solid tumors, leading to p53-dependent cell-cycle arrest and/or apoptosis. At well-tolerated dose schedules, SAR405838 achieves either durable tumor regression or complete tumor growth inhibition in mouse xenograft models of SJSA-1 osteosarcoma, RS4;11 acute leukemia, LNCaP prostate cancer, and HCT-116 colon cancer. Remarkably, a single oral dose of SAR405838 is sufficient to achieve complete tumor regression in the SJSA-1 model. Mechanistically, robust transcriptional upregulation of PUMA induced by SAR405838 results in strong apoptosis in tumor tissue, leading to complete tumor regression. Our findings provide a preclinical basis upon which to evaluate SAR405838 as a therapeutic agent in patients whose tumors retain wild-type p53. *Cancer Res; 74(20); 5855–65. ©2014 AACR.*

Introduction

Although the tumor suppressor function of p53 can be inactivated through gene mutation or deletion (1), p53 is rarely mutated in some forms of human cancer, and this suggests alternative mechanisms for inhibition of the p53 function. The oncoprotein murine double minute 2 (MDM2) is a primary inhibitor of wild-type p53 (2–5). Upon direct binding, MDM2 induces degradation of p53 by functioning as an E3 ligase and blocks the p53 transactivation domain, rendering p53 ineffective as a transcriptional factor (2–5). MDM2 is overexpressed in many types of human cancers through either gene amplification or other mechanisms (6) and contributes to oncogenesis.

Activation of the powerful p53 tumor suppressor function by blocking the MDM2–p53 interaction using small-molecule MDM2 inhibitors is being intensely pursued as a new cancer therapeutic strategy (7–14).

We have previously reported the design of MI-219 as a potent MDM2 inhibitor (8). Although MI-219 demonstrates clear mechanism-based antitumor activity *in vitro* and *in vivo* and is well tolerated in extensive toxicity evaluations in animals, it is not suitable for clinical development. In particular, high doses (300 mg/kg) and an intense schedule (twice daily) are needed for MI-219 to achieve strong antitumor activity *in vivo*. Our optimization efforts have resulted in the discovery of MI-77301 (SAR405838; Fig. 1A), a highly potent and selective MDM2 inhibitor with much improved potency and efficacy over MI-219. We report herein our extensive preclinical characterization of SAR405838.

Materials and Methods

Chemical synthesis of SAR405838

SAR405838 was synthesized using a procedure similar to that used for MI-888 (15) and its purity is >95% by high-performance liquid chromatography.

Biochemical binding assays

Binding affinities of MDM2 inhibitors and p53 peptide (residues 13–29) to MDM2 protein were determined using an

[1]University of Michigan Comprehensive Cancer Center, University of Michigan, Ann Arbor, Michigan. [2]Department of Internal Medicine, University of Michigan, Ann Arbor, Michigan. [3]Department of Pharmacology, University of Michigan, Ann Arbor, Michigan. [4]Department of Medicinal Chemistry, University of Michigan, Ann Arbor, Michigan. [5]Sanofi Oncology, Vitry-sur-Seine, France. [6]Life Sciences Institute, University of Michigan, Ann Arbor, Michigan.

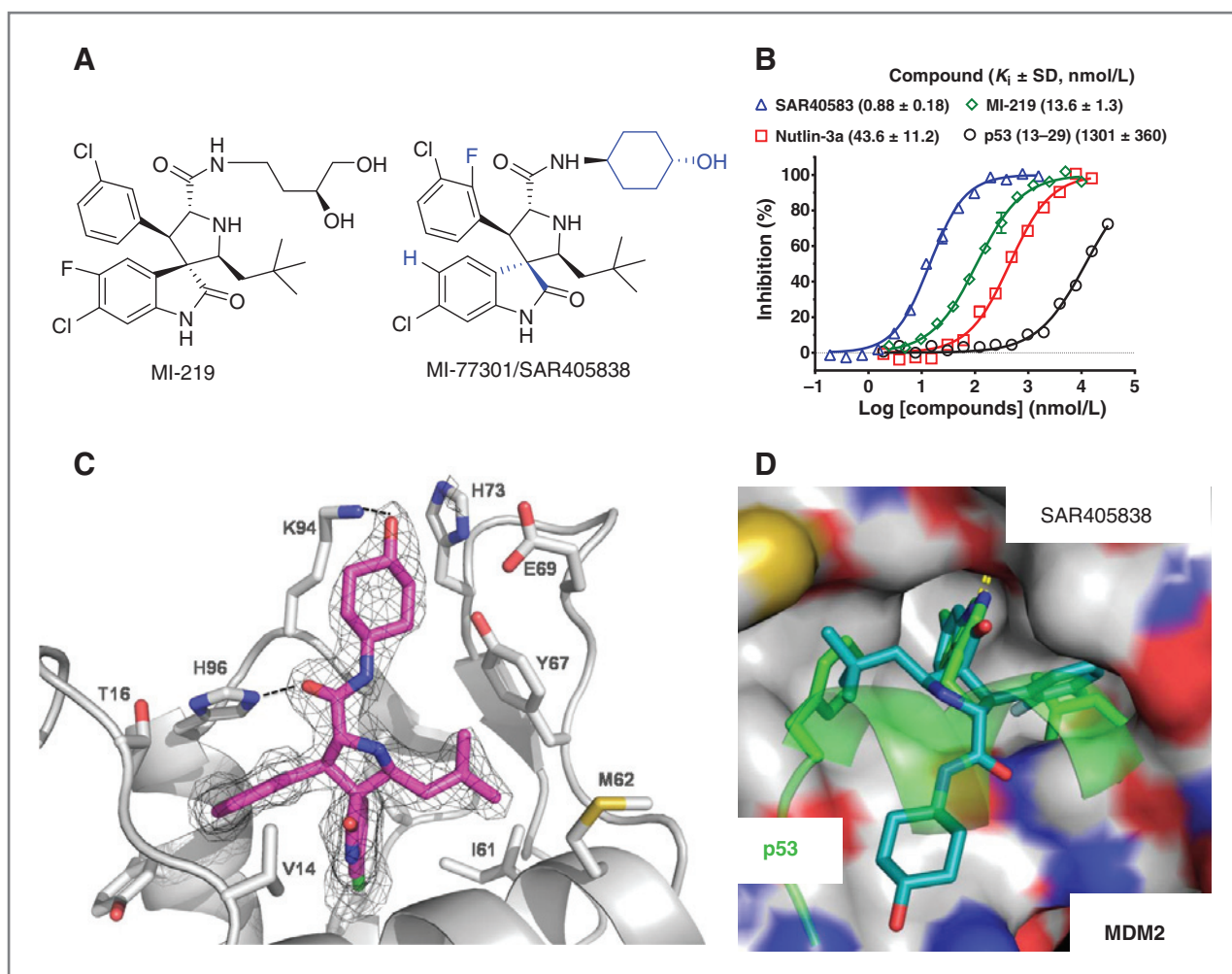*American Association for Cancer Research*

Figure 1. A, chemical structures of SAR405838 and MI-219. B, affinities of SAR405838 and control compounds to human MDM2 protein, determined in a fluorescence-polarization binding assay. C, cocrystal structure of SAR405838/MDM2 at 2.1 Å resolution. D, superposition of SAR405838/MDM2 and p53 peptide/MDM2 cocrystal structures.

FP binding assay (15). Binding affinities of SAR405838 to Bcl-2, Bcl-xL, Mcl-1, and β-catenin were determined using our published methods (16, 17), and its binding affinity to MDMx was determined using Biolayer Interferometry technology (18).

Determination of the cocrystal structure of SAR405838/MDM2 complex

Cocrystals of human MDM2 (10-118) protein with SAR405838 were obtained from the Qiagen Ammonium Sulfate Screen condition B8 at 20°C. Diffraction data were collected at the Advanced Photon Source at Argonne National Laboratory and processed with HKL2000 (19). The cocrystal structure was solved by molecular replacement in Phaser (20) using a structure of MDM2 developed in-house as the search model, fit and refined using Coot (21), and further refined using Buster (22). Details are provided in Supplementary Table S1.

Cell lines, cell growth, cell cycle, cell death, and apoptosis

Unless otherwise stated, all cell lines were purchased directly from ATCC. HCT-116 p53$^{+/+}$ and p53$^{-/-}$ cell lines

were obtained from Dr. Bert Vogelstein, Johns Hopkins University School of Medicine, Baltimore, MD. Cell growth inhibition activity was determined in a water-soluble tetrazolium–based assay (23). Cell-cycle analysis was performed by flow cytometric analysis of DNA content after propidium iodide staining, with cell clumps, doublets, and subdiploid cells excluded from the analysis. Cell death was measured by Trypan blue staining and apoptosis was determined using an Annexin V-FLUOS staining kit (Roche Applied Science).

Real-Time PCR

cDNA was synthesized using a High Capacity cDNA Reverse Transcription Kit (Applied Biosystems) with Oligo dt (Euro-gentech). Next, TaqMan gene expression assays were performed by gene-specific primer/probe sets (Applied Biosystems) for real-time PCR amplification in an Applied Biosystems 7900 thermocycler. *RPL37a* was used for normalization using probes and primers from Applied Biosystems. Relative quantification of mRNA was calculated by a comparative cycle threshold (C_t) method.

Western blotting

For tumor cell lines, the following primary antibodies were used: PUMAα/β (sc-374223) and MDM2 (SMP-14, sc-965) from Santa Cruz Biotechnology; p53 (DO-1, OP43) and MDM2 (OP46) from Millipore; p21 (DCS60), caspase-3 (8G10), and PARP (46D11) from the Cell Signaling Technology. For tumor tissues, the following antibodies were used: p53 (OP43; Millipore), MDM2 (sc-965; Santa Cruz Biotechnology), p21 (556431; BD Biosciences), PARP (9542; Cell Signaling Technology), caspase-3 (AAP-113; Stressgen Bioreagents), and horseradish peroxidase–conjugated GAPDH (sc-5778; Santa Cruz Biotechnology).

Immunohistochemical staining

For immunohistochemistry, the following antibodies were used: p53 (OP43, EMD Millipore) and cleaved caspase-3 (9664; Cell Signaling Technology). p53 was detected by VECTOR Red Alkaline Phosphatase Substrate Kit (AK-5100, Vector) and cleaved caspase-3 was detected by diaminobenzidine (DAB) tetrahydrochloride substrate using a DAB/buffer system (Sigma).

RNA interference and shRNA knockdown

To downregulate PUMA, ON-TARGETplus SMARTpools for human BBC3 (encoding PUMA) and nontargeting negative control siRNAs (Dharmacon) were used. Transfection was performed using Lipofectamine RNAiMAX (Invitrogen). SJSA-1 cells were transfected with siRNAs for 2 days, followed by drug treatment.

For stable p53 knockdown, a 19-bp shRNA interference, corresponding to p53 nucleotides 611–629 (Genbank NM000546; ref. 24) was used, with a scrambled shRNA construct as the control (24). The oligonucleotides were annealed and ligated into a self-inactivating lentiviral vector under the control of the H1 promoter (19) with the GFP reporter gene under control of the human ubiquitin-C promoter. Lentiviral shRNA virus–containing supernatant was used to infect the cells. At 96 hours postinfection, the cells were sorted for GFP fluorescence.

Meso Scale Discovery protein immunoassays

Total protein concentrations were determined with the BCA protein assay kit (Thermo Scientific) and protein analysis was performed by Meso Scale Discovery assays after appropriate dilutions with the following kits: MDM2 (K152FID), p21 (N45ZA-1), p53, cleaved caspase-3 and cleaved PARP (K15102D-1) with a Sector Imager 2400. Results were normalized with total protein concentration.

In vivo microPET and apoptosis imaging

MicroPET scans were done using the microPET FOCUS 120 PET scanner (Siemens Preclinical Solutions). 3′-Deoxy-3′-[(18) F]fluorothymidine(FLT)-positron emission tomography (PET) imaging was performed on isoflurane-anesthetized mice starting 60 minutes after an i.v. injection of 6 to 8 mBq of FLT. Image acquisition time was 12 minutes. Images were reconstructed using a two-dimensional ordered subset-expectation maximization reconstruction algorithm (OSEM2D). Standardized uptake value was calculated for each tumor with three mice/tumors in each group.

In vivo apoptosis induction was assessed by fluorescence molecular tomography imaging performed with FMT2500 (PerkinElmer). Annexin-Vivo-750 uptake scans were done on Ketamine/Xylazine 120/6 mg/kg i.p. anesthetized mice starting at least 4 hours after probes i.v. injection. Images were reconstructed and analyzed using TrueQuant software.

In vivo pharmacodynamic and efficacy experiments

To develop xenograft tumors, 5×10^6 tumor cells with 50% Matrigel were injected subcutaneously on the dorsal side of SCID mice (LNCaP in males and other three models in females).

For pharmacodynamic studies, when tumors reached a mean of 200 mm³, three mice per group were treated with vehicle control or a single dose of the drug via oral gavage and sacrificed at each time point, with tumor tissue harvested for analyses.

For in vivo efficacy experiments, when tumors reached 100 to 200 mm³, mice were randomized into groups of eight mice, except in the HCT-116 and single-dose SJSA-1 efficacy experiments, in which six mice per group were used. Vehicle control (10% PEG400: 3% Cremophor: 87% PBS, or 2%TPGS:98%PEG200) or SAR405838 was given orally once per day for the indicated dose and duration. Tumor sizes and animal weights were measured two to three times per week with tumor volume (mm³) = (length $\times$ width²)/2. Statistical analyses were done by two-way ANOVA and unpaired two-tailed t test, using Prism (version 4.0, Graph-Pad). All animal experiments were performed under the guidelines of the University of Michigan Committee for Use and Care of Animals or of the Sanofi Committee for Use and Care of Animals.

Results

SAR405838 has a much improved binding affinity to MDM2 and chemical stability over MI-219 and good oral pharmacokinetics in animals

SAR405838 has several major structural differences from MI-219: a different stereochemistry in the quaternary carbon atom, different halogen substitution patterns in both phenyl rings, and a conformationally constrained cyclohexanol group (Fig. 1A).

SAR405838 has $K_i = 0.88$ nmol/L to human MDM2 protein in a competitive binding assay (15) and is >10, >50, and >1,000 times more potent than MI-219, nutlin-3a, and the p53 peptide, respectively (Fig. 1B). To assess its selectivity, we tested SAR405838 for binding to MDMx, a homolog of MDM2. We also tested SAR405838 for its binding to Bcl-2, Bcl-xL, Mcl-1 (25, 26), and β-catenin (17, 27), all of which contain a hydrophobic binding groove on their surface. SAR405838 shows no appreciable binding to these proteins at concentrations as high as 10 μmol/L (Supplementary Fig. S1). SAR405838 has IC$_{50}$ values in the μmol/L range at best, for only a few of the >200 receptors/enzymes tested (data not shown). SAR405838 was tested for its stability in cell culture media and two other solutions in which some spiro-oxindoles were shown to isomerize (15) and was found to be stable (Supplementary Fig. S2). It has good oral pharmacokinetics in mice, rats, and dogs (Supplementary Table S3).
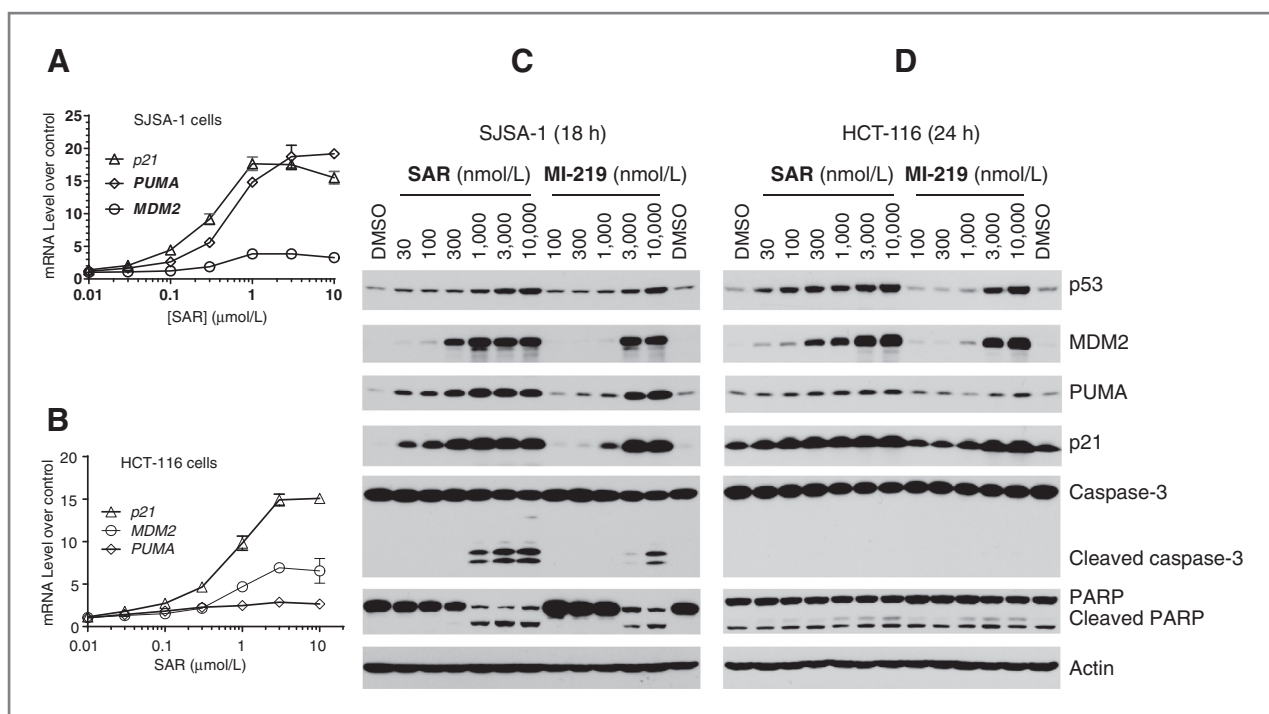
Figure 2. SAR405838 potently activates p53 in the SJSA-1 and HCT-116 cancer cell lines and strongly induces PUMA upregulation and cleavage of caspase-3 and PARP in the SJSA-1 cell line but not in the HCT-116 cell line. A and B, analysis of dose-dependent transcriptional induction of p21, MDM2, and PUMA in both cell lines. C and D, analysis of dose-dependent induction of p53, p21, MDM2, and PUMA proteins and cleavage of caspase-3 and PARP in both cell lines.

Hence, SAR405838 is a potent and selective MDM2 inhibitor with good chemical stability and excellent oral bioavailability.

Structural basis of the high affinity binding of SAR405838 to MDM2

We determined the cocrystal structure of the SAR405838/MDM2 complex at 2.1 Å resolution (Fi. 1C and Supplementary Table S1). SAR405838 mimics the three key p53-binding residues (Phe19, Trp23, and Leu26; Fig. 1D; ref. 28) in its interaction with MDM2, but captures additional interactions. The Cl atom in the oxindole group of SAR405838 has extensive hydrophobic contacts with MDM2. There is π-π stacking between the His96 of MDM2 and the 2-fluoro-3-chlorophenyl in SAR405838 and a hydrogen bond between the imidazole side chain of His96 and the carboxyl group in SAR405838. Interestingly, the N-terminus of MDM2 (residues 10–18) refolds and enjoys extensive interactions with SAR405838 through Val14 and Thr16, different from those in the p53:MDM2 (28) and nutlin:MDM2 (7) cocrystal structures.

To investigate the significance of this refolding, we tested the binding affinities of SAR405838 to several shorter MDM2 proteins (Supplementary Table S2). Removal of the first 9 N-terminal residues in MDM2 has no effect on binding to SAR405838, but further truncation reduces the binding affinity. SAR405838 binds to MDM2 18-118 and 25-118 proteins with K_i = 8.6 nmol/L and 24.0 nmol/L, respectively, being 10 and 25 times weaker than that with the MDM2 1-118 protein. The p53 peptide (13–29) binds to MDM2 25-118 protein with a higher affinity (K_i = 283 nmol/L) than to MDM2 1-118 protein (K_i = 1.3

μmol/L) and nutlin-3a binds to these two MDM2 constructs (1-118 and 25-118) with similar affinities. These data show that residues 10–24 in MDM2 enhance the binding affinity for SAR405838 by a factor of 25, but have no effect for the binding to p53 peptide or to nutlin-3a.

SAR405838 potently activates the p53 pathway

Mechanistically, by occupying the p53 pocket in MDM2 (Fig. 1C), an MDM2 inhibitor blocks p53–MDM2 interaction and consequently the MDM2-mediated p53 protein degradation, leading to p53 accumulation and transcriptional activation in cells with wild-type p53 but not in cells with mutated or deleted p53 (7, 8). Activation of p53 will transcribe its targeted genes, such as *MDM2* and *p21*, while having no effect on p53 transcription (7, 8). We analyzed SAR405838 for its activity and specificity to activate p53, using MI-219 and/or nutlin-3a as controls.

In the SJSA-1 osteosarcoma cell line with wild-type p53 and *MDM2* gene amplification, SAR405838 induces dose-dependent upregulation of MDM2, p21, and PUMA mRNA with EC_{50} values of 0.3 to 0.6 μmol/L (Fig. 2A), but has no effect on p53 mRNA (Supplementary Fig. S3). In the HCT-116 colon cancer cell line with wild-type p53 and no *MDM2* gene amplification, SAR405838 also induces a robust, dose-dependent increase of MDM2 and p21 mRNA, with EC_{50} values of 0.7 μmol/L (Fig. 2B), but no increase of p53 mRNA (Supplementary Fig. S3). However, SAR405838 only induces a modest increase (∼3-fold at 1 and 3 μmol/L) of PUMA mRNA in the HCT-116 cells, in contrast to 19-fold induction at 1 μmol/L in the SJSA-1 cells

Table 1. SAR405838 potently inhibits cell growth in cancer cell lines of diverse tumor types with wild-type p53 and displays high selectivity over cancer cell lines with mutated or deleted p53

Cell lines	p53 Status	Cell growth inhibition (IC$_{50}$, μmol/L)		
		SAR405838	MI-219	Nutlin-3a
SJSA-1	Wild-type	0.092 ± 0.019	1.4 ± 0.2	1.3 ± 0.2
RS4;11	Wild-type	0.089 ± 0.027	1.0 ± 0.2	0.57 ± 0.13
LNCaP	Wild-type	$0.27 \pm 0.0\ 3$	1.1 ± 0.1	1.2 ± 0.4
HCT-116	Wild-type	0.20 ± 0.04	0.95 ± 0.05	0.86 ± 0.11
HCT-116 (p53$^{-/-}$)	Deletion	>20	>10	>10
SAOS-2	Deletion	>10		
PC-3	Deletion	>10		
SW620	Mutation	>10		

(Fig. 2A). In both cell lines, SAR405838 is 5 to 10 times more potent than MI-219 and nutlin-3a in induction of p21 and MDM2 transcription (Supplementary Fig. S3).

Western blotting showed that SAR405838 induces a dose-dependent increase in the levels of p53, p21, and MDM2 proteins in both SJSA-1 and HCT-116 cell lines (Fig. 2C). While SAR405838 induces clear increase of PUMA protein at 30 nmol/L in the SJSA-1 cell line, it only has a modest effect on PUMA in the HCT-116 cell line even at 10 μmol/L (Fig. 2C). SAR405838 also dose dependently increases the levels of p53, p21, MDM2, and PUMA proteins in the RS4;11 acute leukemia and LNCaP prostate cancer cell lines, with a clear effect at 100 nmol/L (Supplementary Fig. S4). SAR405838 is >10 times more potent than MI-219 in activation of p53 in these four cell lines (Fig. 2C–D and SI Fig. S4).

We tested the specificity of SAR405838 in cancer cell lines with mutated or deleted p53 (7, 8). SAR405838 has no effect on p21, MDM2, PUMA, and p53 proteins in cancer cell lines harboring mutated p53 or with p53 deletion (Supplementary Fig. S5), indicating its high cellular specificity.

Taken together, our cellular data provide clear evidence that SAR405838 is a potent and specific MDM2 inhibitor.

SAR405838 potently inhibits cell growth and induces cell-cycle arrest and/or apoptosis in cancer cell lines in a p53-dependent manner

SAR405838 is 5 to 10 times more potent than MI-219 and nutlin-3a in inhibition of cell growth in wild-type p53 cancer cell lines of diverse tumor types (Table 1). SAR405838 has IC$_{50}$ ≥10 μmol/L against all cancer cell lines with a mutated or deleted p53 (Table 1), showing high specificity.

Activation of p53 by nutlin-3a results in cell-cycle arrest in all cancer cell lines investigated, but provokes apoptosis only in some cancer cell lines (29). We evaluated by flow cytometry, the effect of SAR405838 on cell-cycle progression and apoptosis in four cancer cell lines with wild-type p53 (Fig. 3A and B). In the SJSA-1 cell line, SAR405838 induces both cell-cycle arrest and apoptosis in a dose-dependent manner, but displays different kinetics for these two cellular processes, with an early onset for cell-cycle arrest and a late onset for apoptosis. In the RS4;11 acute leukemia cell line, SAR405838 induces time- and dose-dependent apoptosis but not cell-cycle arrest. In the LNCaP

prostate cancer and HCT-116 colon cancer cell lines, SAR405838 effectively inhibits cell-cycle progression at 0.3 μmol/L or higher with 24-hour treatment, but has a modest or minimal effect on apoptosis induction even at 10 μmol/L.

Using the HCT-116 p53$^{+/+}$ and the isogenic p53$^{-/-}$ cell lines, we showed that the cellular growth inhibitory activity of SAR405838 is p53-dependent (Table 1). To determine whether the cellular activity of SAR405838 is also strictly p53-dependent in the SJSA-1, RS4;11, and LNCaP cell lines, we stably knocked down p53 by shRNAi. Efficient knockdown of p53 in SJSA-1 cells effectively attenuates upregulation of p53, p21, MDM2, and PUMA, as well as cleavage of PARP and caspase-3 (Fig. 3C) by SAR405838, reduces its potency in cell growth inhibition by >20 times, and disables its ability to induce apoptosis (Fig. 3C) and cell-cycle arrest (Supplementary Fig. S6). Knockdown of p53 also effectively attenuates cell growth inhibition and apoptosis induction by SAR405838 in the RS4;11 cell line (Supplementary Fig. S7) and cell growth inhibition and cell-cycle arrest in the LNCaP line by SAR405838 (Supplementary Fig. S8). These data firmly establish that the cellular activity of SAR405838 is p53-dependent.

PUMA mediates apoptosis induction by SAR405838 in tumor cells

Although SAR405838 can robustly activate p53 in both the SJSA-1 and HCT-116 cell lines, it selectively induces apoptosis in the SJSA-1 cells. As SAR405838 effectively increases the mRNA and protein levels of PUMA in SJSA-1 cells, but not in HCT-116 cells, we examined the role of PUMA, a strong proapoptotic protein (30). While efficient knockdown of PUMA by siRNA in SJSA-1 cells has no effect on induction of p53, p21, and MDM2 proteins by SAR405838, it effectively reduces the cleavage of caspase-3 and apoptosis by SAR405838 (Fig. 3D).

In addition to PUMA, p53 can also directly regulate the expression of proapoptotic Bax and Noxa (31, 32), both of which play a role in p53-mediated apoptosis (33). Real-time quantitative reverse transcription PCR (qRT-PCR) analysis, however, showed that SAR405838, MI-219 and nutlin-3a have no significant effect on the mRNA levels of Bax and Noxa in the SJSA-1 cell line (Supplementary Fig. S3). Hence, our data show that PUMA plays a key role in apoptosis induction by SAR405838 in SJSA-1 cells.
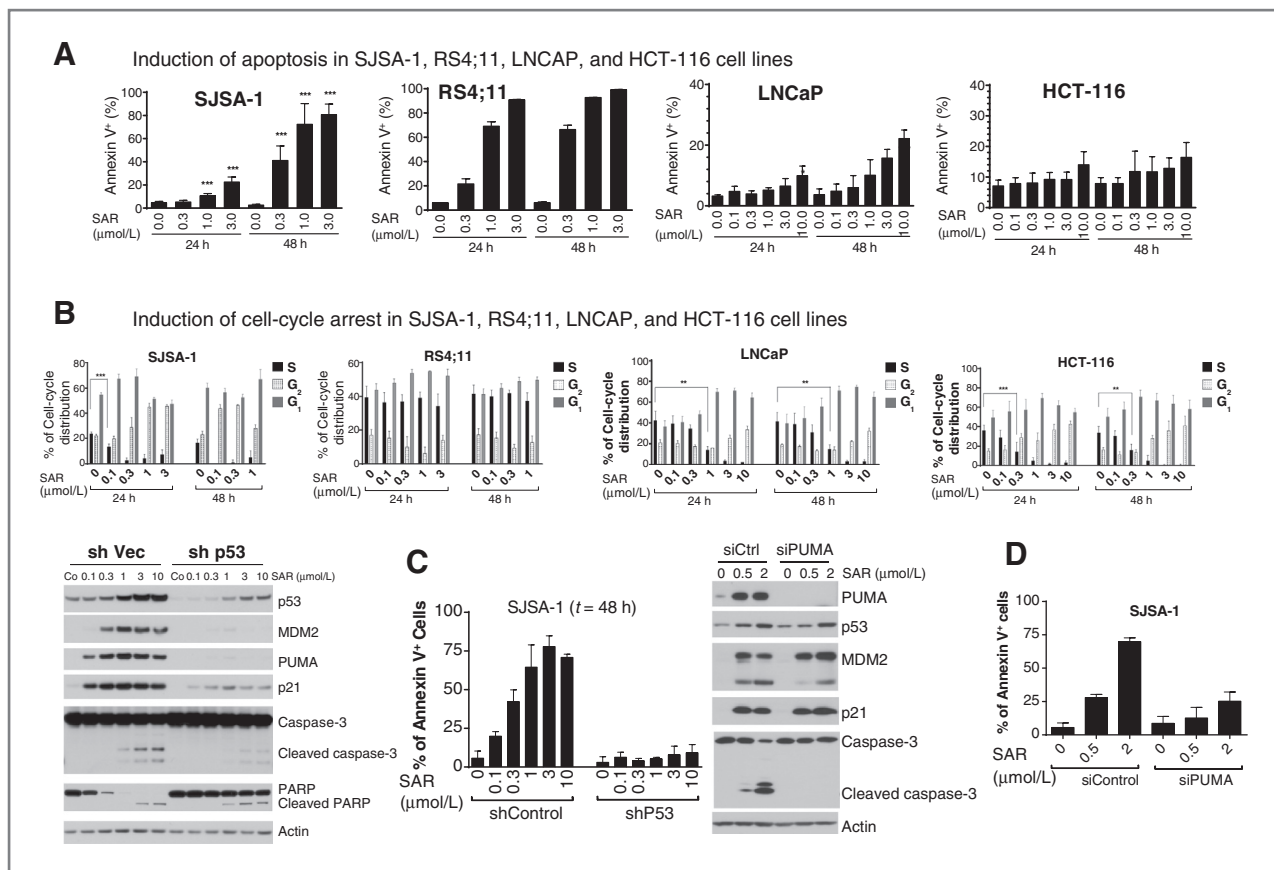
Figure 3. SAR405838 induces p53-dependent cell-cycle arrest and/or apoptosis in SJSA-1 RS4;11, LNCaP, and HCT-116 cancer cell lines. A, analysis of apoptosis induction in the four cell lines. B, analysis of cell-cycle progression in four cell lines. C, investigation of the role of p53 in apoptosis induction by SAR405838. D, examination of the role of PUMA in apoptosis induction by SAR40583 in the SJSA-1 cell line.

SAR405838 strongly activates p53 in tumor tissues

To gain insights into the mechanism of action of SAR405838 *in vivo*, we performed pharmacodynamic analyses in the SJSA-1, HCT-116, RS4;11, and LNCaP xenograft tumors in mice treated with a single, oral dose of SAR405838.

In the SJSA-1 tumor tissue, qRT-PCR analysis showed that SAR405838 induces dose-dependent and robust upregulation for p21 and PUMA mRNA, but a relatively moderate increase for MDM2 mRNA (Fig. 4A). Induction for p21 and PUMA mRNA is already robust at 6 hours at all doses tested and the strong effect persists longer with higher doses, increasing from 24 hours with 50 mg/kg to 72 hours with 200 mg/kg (Fig. 4A). On the protein level, SAR405838 induces dose-dependent increases of MDM2, p21, and p53 proteins at both 6-hour and 24-hour time points (Fig. 4B). However, unlike the kinetics observed for transcriptional induction, the protein level for each of MDM2, p21, and p53 peaks at 6 hours at all three doses and is minimally elevated at 72 hours (Fig. 4B). Immunohistochemical (IHC) staining confirmed that the p53 protein is strongly upregulated at 3 and 6 hours but greatly diminished at 24 hours in tumor tissue (Fig. 4C). Compared with upregulation of p53, MDM2, and p21 proteins, cleavage of caspase-3 is a delayed event, minimal at 6 hours, with all the three doses but very robust at 24 hours (Fig. 4B). Western blotting showed that

cleavage of PARP and caspase-3 was very clear at 24 hours in the tumor tissue treated with a single dose of SAR405838 at 100 mg/kg (Supplementary Fig. S9). These *in vivo* pharmacodynamic data indicate that SAR405838 induces dose- and time-dependent p53 activation and strong apoptosis in the SJSA1 tumor tissue.

In HCT-116 xenograft tumor tissue, SAR405838 induces dose- and time-dependent transcription of *p21*, *PUMA*, and *MDM2* genes (Supplementary Fig. S11A). However, the magnitude of induction of p21 and MDM2 mRNA by SAR405838 is three to four times lower than that observed in the SJSA-1 tumor tissue. More strikingly, the maximum induction of PUMA mRNA by SAR405838 is only 3-fold over the control even at 200 mg/kg, as compared with the >40-fold increase in the SJSA-1 tumor tissue. On the protein level, SAR405838 dose dependently increases MDM2, p21, and p53 proteins in the HCT-116 tumor tissue with kinetics similar to those in the SJSA-1 tumor (Supplementary Fig. S10B). However, SAR405838 induces minimal caspase-3 cleavage in the HCT-116 tumor in all doses and at all time points.

In the RS4;11 xenograft tissue, SAR405838 induces dose-dependent transcriptional upregulation of MDM2, p21, and PUMA mRNA (Supplementary Fig. S11A), similar to that observed in the SJSA-1 xenograft tissue. Strong apoptosis induction was evident at 100 and 200 mg/kg and 6 and 24
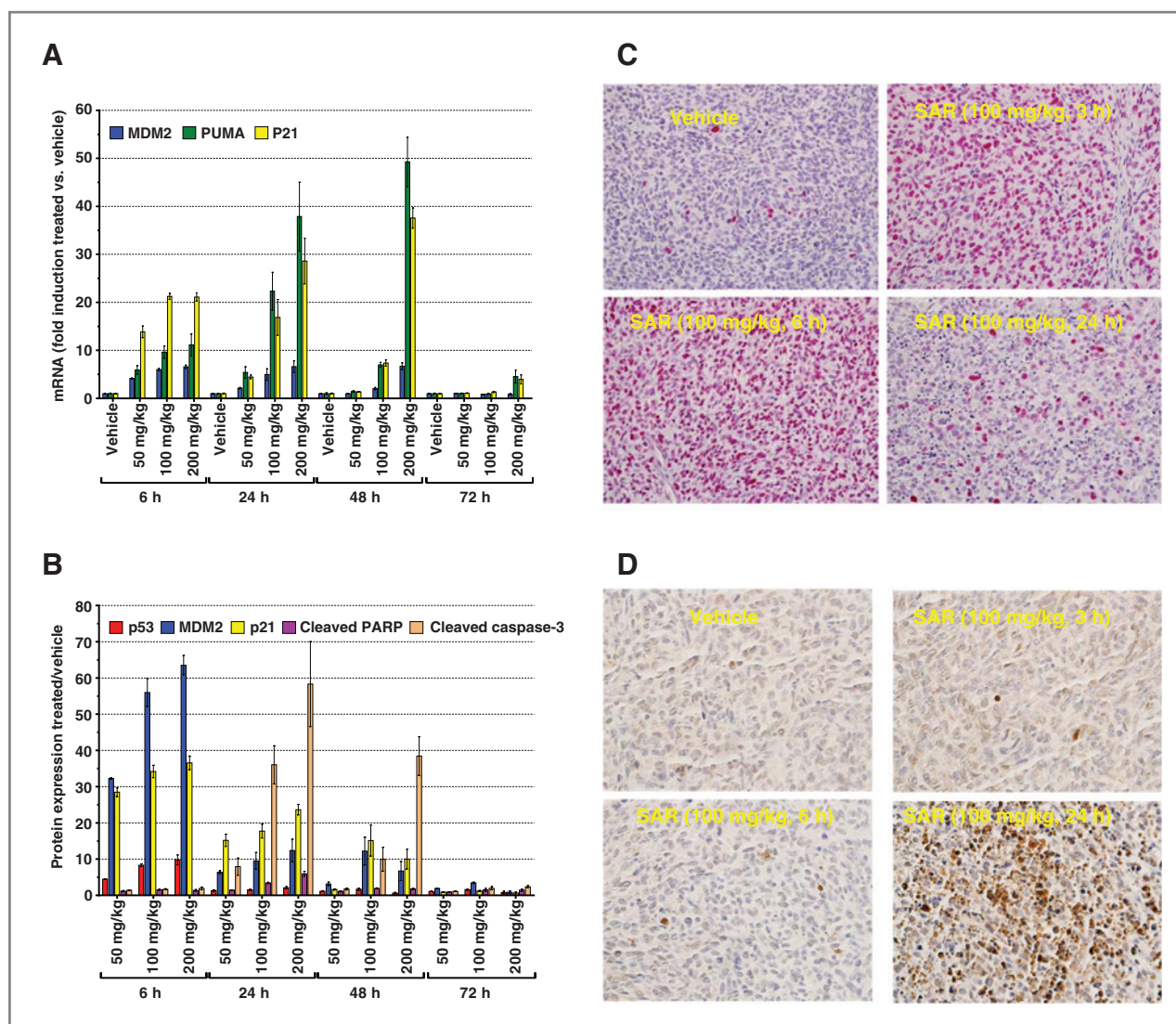
Figure 4. SAR405838 strongly activates p53 and induces apoptosis in SJSA-1 xenograft tumors in mice. A, qRT-PCT analysis of mRNA induction of MDM2, p21, and PUMA by SAR405838 at different doses and time points in SJSA-1 tumor tissue. B, Mesoscale analysis of induction of p53, p21, MDM2, cleaved caspase-3, and cleaved PARP with a single dose of SAR405838 at different doses and time points in SJSA-1 tumor tissue. C, IHC staining of p53 in SJSA-1 tumor tissue. D, IHC staining of cleaved caspase-3 in SJSA-1 tumor tissue.

hours based upon cleavage of caspase-3 and PARP (Supplementary Fig. S11B).

In the LNCaP xenograft tissue, SAR405838 induces dose- and time-dependent transcriptional upregulation of MDM2, p21, and PUMA (Supplementary Fig. S12A). The magnitude of the transcriptional upregulation with p21 and MDM2 was similar to that observed in the other three models. The induction of PUMA mRNA by SAR405838 in the LNCaP tumor tissue is weaker than in the SJSA-1 and RS4;11 tumor tissues, but stronger than in the HCT-116 tumor tissue. On the protein level, SAR405838 induces robust accumulation of MDM2, p21, and p53 in a time- and dose-dependent manner (Supplementary Fig. S12B). While the level of p53 protein peaks at the 6-hour time point, the strong upregulation of p21 and MDM2 proteins persists much longer. There is, however, a minimal

amount of cleaved caspase-3 in the LNCaP tumor tissue (Supplementary Fig.S11B), indicating a low level of apoptosis induction.

Hence, in all the four models examined, a single, oral dose of SAR405838 activates p53 in tumor tissues in a dose- and time-dependent manner and is capable of inducing strong apoptosis in the SJSA-1 and RS4;11 xenograft tumors, but only minimal or modest apoptosis in the HCT-116 and LNCaP xenograft tumors.

SAR405838 achieves complete and durable SJSA-1 tumor regression

We tested the efficacy of SAR405838 in the SJSA-1 xenograft model, which has *MDM2* gene amplification and has been used to evaluate other MDM2 inhibitors *in vivo* (7, 8, 34, 35).
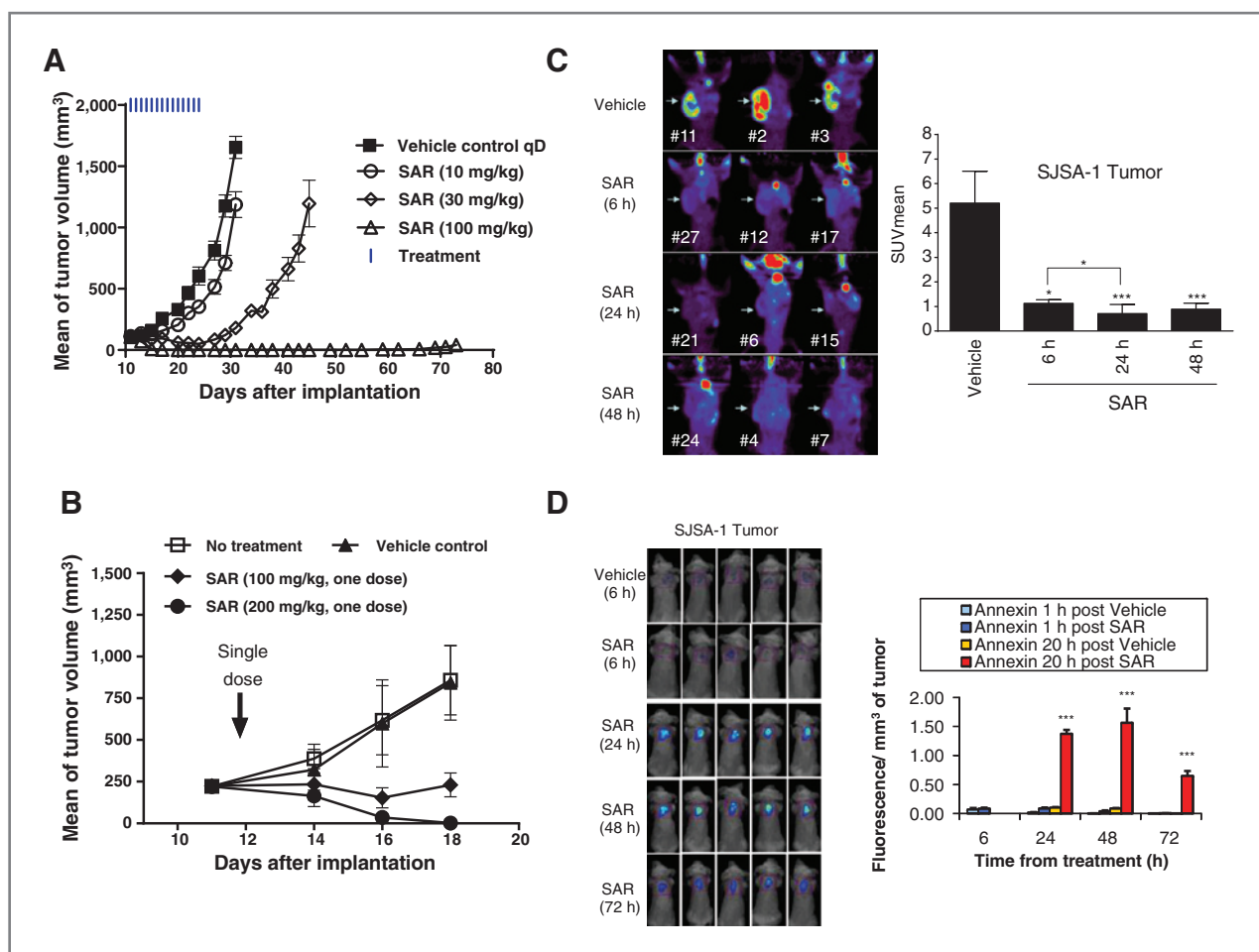
Figure 5. SAR405838 induces strong apoptosis and achieves complete tumor regression in the SJSA-1 osteosarcoma xenograft model. A, antitumor activity of SAR405838, with daily dosing for 2 weeks. B, antitumor activity of a single-dose of SAR405838. C, FLT-PET imaging analysis of cell proliferation in the SJSA-1 tumor tissue. D, enhanced fluorescent Annexin-V imaging uptake analysis of apoptosis in the SJSA-1 tumor tissue.

With daily, oral administration for 2 weeks, SAR405838 at 10 mg/kg has no significant activity but at 30 mg/kg, it induces partial tumor regression (Fig. 5A). At 100 mg/kg, it achieves rapid, complete, and persistent tumor regression (Fig. 5A). After only four doses, the average tumor volume shrinks by >90% and after 9 doses, all tumors completely regress, becoming undetectable. The complete tumor regression is durable; 31 days after the last dose, at day 55, all eight mice remain tumor free, and at day 73, 2 months after the last dose, 5 of 8 (63%) of the animals are still tumor free.

As a single dose of SAR405838 induces strong apoptosis in the SJSA-1 tumor tissue, we tested whether a single, oral dose of SAR405838 can achieve strong antitumor activity (Fig. 5B). Remarkably, a single 100 mg/kg oral treatment with SAR405838 effectively inhibits tumor growth and a single oral dose of 200 mg/kg induces complete tumor regression in 100% of the mice.

To gain further insights into the complete tumor regression achieved with a single dose of SAR405838 in the SJSA-1 tumor model, we used the FLT-PET technique to image tumor proliferation (Fig. 5C) and an Annexin-V 750 kit to image tumor apoptosis in mice. The imaging data showed that a single dose of SAR405838 effectively inhibits tumor cell proliferation and induces strong apoptosis, with the effect persisting for 72 hours (Fig. 5D).

SAR405838 is highly efficacious in xenograft models of multiple tumor types lacking *MDM2* gene amplification

As *MDM2* gene amplification is only found in, on average, 5% to 7% of human tumors (6), we tested SAR405838 in RS4;11, LNCaP, and HCT-116 tumor models, which have a wild-type p53 status but that all lack *MDM2* gene amplification.

SAR405838 achieves partial tumor regression at 50 mg/kg and complete tumor regression at 100 or 200 mg/kg daily dosing in the acute lymphoblastic leukemia RS4;11 model (Fig. 6A). The tumor regression achieved by SAR405838 at 200 mg/kg in the RS4;11 model is durable; at day 71, 25 days after the last dose, all eight mice remained tumor free.

SAR405838 shows strong antitumor activity in the LNCaP prostate cancer model (Fig. 6B). Administered daily at 50 mg/kg for 4 weeks, it inhibits tumor growth by 70%
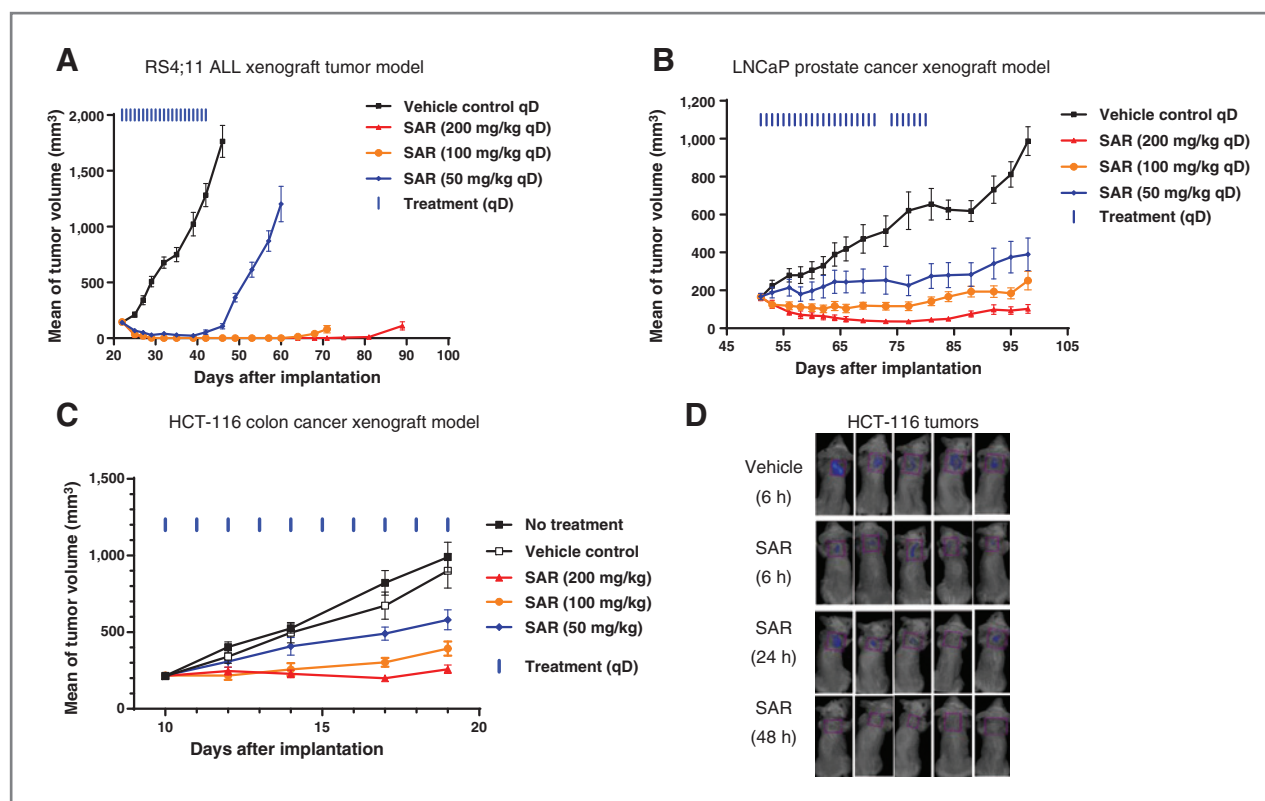
Figure 6. SAR405838 demonstrates strong antitumor activity in RS4;11, LNCaP, and HCT-116 models. A, antitumor activity of SAR405838 in the RS4;11 xenograft model. B, antitumor activity of SAR405838 in the LNCaP xenograft model. C, antitumor activity of SAR405838 in the HCT-116 xenograft model. D, enhanced fluorescent Annexin-V imaging uptake analysis of apoptosis in the HCT-116 tumor tissue.

over the vehicle control, at 100 mg/kg it completely inhibits tumor growth, and at 200 mg/kg, it induces 80% tumor regression.

Although SAR405838 fails to achieve tumor regression in the HCT-116 colon cancer model, it effectively inhibits tumor growth (Fig. 6C). SAR405838 at 100 mg/kg daily dosing inhibits tumor growth by >80% over the vehicle control at the end of the treatment, and at 200 mg/kg, completely inhibits tumor growth. Annexin-V *in vivo* imaging consistently showed that SAR405838 does not induce detectable apoptosis in the HCT-116 tumor tissue in mice (Fig. 6D).

SAR405838 is well tolerated in these efficacy experiments, producing less than 10% weight loss in all dose-scheduled tests (Supplementary Fig. S13), and causing no signs of toxicity in mice.

Discussion

Our extensive optimization of MI-219 has yielded SAR405838, which is >10 times more potent than MI-219 in binding to MDM2 and in activation of p53 in tumor cells with wild-type p53. Importantly, SAR405838 has good chemical stability in solution, thus overcoming a significant issue associated with our earlier MDM2 inhibitors (36). SAR405838 has good oral pharmacokinetics in rodents and nonrodents and achieves much stronger and more sustained p53 activation than MI-219 in tumor tissues with oral administration. This

translates into an impressive antitumor activity for SAR405838, including complete and persistent tumor regression with oral, daily administration in the SJSA-1 tumor model. Remarkably, a single, oral dose of SAR405838 at 200 mg/kg is capable of achieving complete SJSA-1 tumor regression in 100% of mice. Although genetic studies have shown that tissue-specific p53 activation by the deletion of the *MDM2* gene results in complete regression of established tumors (37–39), previously reported MDM2 inhibitors, including MI-219, nutlin-3a, and recently reported more potent MDM2 inhibitors, such as AM-8533 (34) and RG-7112 (35), all fail to achieve complete tumor regression in the SJSA-1 tumor model. Consistently, *in vivo* imaging showed that a single dose of SAR405838 induces sustained apoptosis persisting for 3 days in SJSA-1 tumors. Although only ~5% of human cancers have an amplified *MDM2* gene (6), a higher frequency of *MDM2* gene amplification occurs in certain tumor types, including soft tissue tumors (20%), osteosarcomas (16%), and esophageal carcinomas (13%), and well-differentiated liposarcomas (>80%; refs. 40, 41). The complete tumor regression achieved by SAR405838 in the SJSA-1 xenograft model suggests its strong therapeutic potential as a single agent for the treatment of human tumors with *MDM2* gene amplification.

SAR405838 also shows strong antitumor activity in xenograft models of different tumor types that possess wild-type p53 but lack *MDM2* gene amplification. SAR405838 achieves

complete tumor regression in the RS4;11 acute leukemia model, partial (80%) tumor regression in the LNCaP prostate cancer model, and complete tumor growth inhibition in the HCT-116 colon cancer model. The tumor regression correlates with the ability of SAR405838 to induce strong apoptosis in tumors. Our data suggest that SAR405838 may also have a therapeutic potential for the treatment of human cancers containing a wild-type p53 but lacking *MDM2* gene amplification.

While SAR405838 induces strong upregulation of p21 and MDM2 in all tested cancer cell lines with wild-type p53, it has a different effect on PUMA *in vitro* and *in vivo*. SAR405838 induces robust upregulation of PUMA in SJSA-1 and RS4;11 tumor cells, but has a modest effect in LNCaP and HCT-116 tumor cells. Furthermore, strong upregulation of PUMA by SAR405838 correlates with apoptosis induction *in vitro* and *in vivo* and complete tumor regression *in vivo*, suggesting the critical role of PUMA in mediating apoptosis and tumor regression. Indeed, knockdown of PUMA by siRNA in SJSA-1 cells effectively reduces activation of caspase-3 and apoptosis induction by SAR405838, without affecting induction of p53, MDM2, and p21 proteins. Although Noxa and Bax are also p53-targeted genes, they are not induced by SAR405838 in SJSA-1 cells. These data suggest that PUMA is a key mediator for apoptosis induction by MDM2 inhibitors in tumor cells and that strong upregulation of PUMA induced by SAR405838 results in complete tumor regression *in vivo*.

The SAR405838:MDM2 cocrystal structure provides insights into the high affinity binding. In addition to capturing all the key hydrogen bonding and hydrophobic contacts between the three p53 key binding residues with MDM2 (28), SAR405838 enjoys several additional interactions with MDM2 that are not observed in the p53:MDM2 (28) or nutlin:MDM2 cocrystal structures (9). In particular, SAR405838 induces refolding of the unstructured extreme N-terminus of MDM2 (residues 10–25), which further enhances their interactions and enhances the binding affinity by 25-fold but makes no significant contribution to the binding of nutlin-3a and the p53 peptide to MDM2.

In summary, our present study demonstrates that SAR405838 is a potent and highly efficacious MDM2 inhibitor. On the basis of these promising preclinical data, SAR405838 was selected for clinical development and is currently being evaluated in clinical trials for the treatment of human cancer.

Disclosure of Potential Conflicts of Interest

Authors' Contributions

Conception and design: S. Wang, C. Barrière, J.A. Stuckey, S. Shangary, S. Yu, L. Besret, S. Guerif, L. Debussche
Development of methodology: S. Wang, Y. Zhao, I. Meaux, L. Liu, S. Shangary, L. Besret, S. Guerif, L. Debussche
Acquisition of data (provided animals, acquired and managed patients, provided facilities, etc.): D. McEachern, I. Meaux, C. Barrière, J.A. Stuckey, J.L. Meagher, L. Bai, L. Liu, C.G. Hoffman-Luca,, J. Lu, A. Aguilar, L. Besret, S. Guerif, P. Pannier, D. Gorge-Bernat
Analysis and interpretation of data (e.g., statistical analysis, biostatistics, computational analysis): S. Wang, Y. Zhao, D. McEachern, I. Meaux, C. Barrière, J.A. Stuckey, J.L. Meagher, L. Bai, L. Liu, J. Lu, S. Yu, D. Bernard, O. Dos-Santos, L. Besret, S. Guerif, L. Debussche
Writing, review, and/or revision of the manuscript: S. Wang, D. McEachern, I. Meaux, C. Barrière, J.A. Stuckey, J.L. Meagher, L. Liu, L. Besret, S. Guerif, L. Debussche
Administrative, technical, or material support (i.e., reporting or organizing data, constructing databases): W. Sun, D. McEachern, J.A. Stuckey, J.L. Meagher, O. Dos-Santos, L. Besret, S. Guerif
Study supervision: S. Wang, C. Barrière, L. Besret, S. Guerif, L. Debussche
Other (design and chemical synthesis of SAR405838): W. Sun

Grant Support

References

1. Hainaut P, Hollstein M. p53 and human cancer: the first ten thousand mutations. Adv Cancer Res 2000;77:81–137.
2. Wu X, Bayle JH, Olson D, Levine AJ. The p53-mdm2 autoregulatory feedback loop. Genes Dev 1993;7:1126–32.
3. Freedman DA, Wu L, Levine AJ. Functions of the MDM2 oncoprotein. Cell Mol Life Sci 1999;55:96–107.
4. Momand J, Wu HH, Dasgupta G. MDM2–master regulator of the p53 tumor suppressor protein. Gene 2000;242:15–29.
5. Bond GL, Hu W, Levine AJ. MDM2 is a central node in the p53 pathway: 12 years and counting. Curr Cancer Drug Targets 2005;5:3–8.
6. Momand J, Jung D, Wilczynski S, Niland J. The MDM2 gene amplification database. Nucleic Acids Res 1998;26:3453–9.
7. Vassilev LT, Vu BT, Graves B, Carvajal D, Podlaski F, Filipovic Z, et al. In vivo activation of the p53 pathway by small-molecule antagonists of MDM2. Science 2004;303:844–8.
8. Shangary S, Qin D, McEachern D, Liu M, Miller RS, Qiu S, et al. Temporal activation of p53 by a specific MDM2 inhibitor is selectively toxic to tumors and leads to complete tumor growth inhibition. Proc Natl Acad Sci U S A 2008;105:3933–8.
9. Vassilev LT. p53 Activation by small molecules: application in oncology. J Med Chem 2005;48:4491–9.
10. Vassilev LT. MDM2 inhibitors for cancer therapy. Trends Mol Med 2007;13:23–31.
11. Shangary S, Wang S. Targeting the MDM2-p53 interaction for cancer therapy. Clin Cancer Res 2008;14:5318–24.
12. Wang S, Zhao Y, Bernard D, Aguilar A, Kumar S. Targeting the MDM2-p53 protein-protein interaction for new cancer therapeutics. Top Med Chem 2012;8:57–80.
13. Carry JC, Garcia-Echeverria C. Inhibitors of the p53/hdm2 protein-protein interaction- Path to the clinic. Bioorg Med Chem Letters 2013;23:2480–5.
14. Zhao Y, Bernard D, Wang S. Small molecule inhibitors of MDM2-p53 and MDMX-p53 interaction as new cancer therapeutics. BioDiscovery 2013;8.

15. Zhao Y, Yu S, Sun W, Liu L, Lu J, McEachern D, et al. A potent small-molecule inhibitor of the MDM2-p53 interaction (MI-888) achieved complete and durable tumor regression in mice. J Med Chem 2013;56:5553–61.

16. Zhou H, Chen J, Meagher JL, Yang CY, Aguilar A, Liu L, et al. Design of Bcl-2 and Bcl-xL Inhibitors with Subnanomolar Binding Affinities Based upon a New Scaffold. J Med Chem 2012;55:4664–82.

17. Kawamoto SA, Thompson AD, Coleska A, Nikolovska-Coleska Z, Yi H, Wang S. Analysis of the interaction of BCL9 with beta-catenin and development of fluorescence polarization and surface plasmon resonance binding assays for this interaction. Biochemistry 2009;48:9534–41.

18. Concepcion J, Witte K, Wartchow C, Choo S, Yao D, Persson H, et al. Label-free detection of biomolecular interactions using BioLayer interferometry for kinetic characterization. Comb Chem High Throughput Screen 2009;12:791–800.

19. Lois C, Hong EJ, Pease S, Brown EJ, Baltimore D. Germline transmission and tissue-specific expression of transgenes delivered by lentiviral vectors. Science 2002;295:868–72.

20. McCoy AJ, Grosse-Kunstleve RW, Adams PD, Winn MD, Storoni LC, Read RJ. Phaser crystallographic software. J Appl Crystallogr 2007;40:658–67.

21. Emsley P, Cowtan K. Coot: model-building tools for molecular graphics. Acta Crystallographica Section D Biolo Crystallogr 2004;60:2126–32.

22. Bricogne G, Blanc E, Brandl M, Flensburg C, Keller P, Paciorek W, et al. BUSTER. Cambridge, United Kingdom: Global Phasing Ltd; 2011.

23. Teodoro JG, Evans SK, Green MR. Inhibition of tumor angiogenesis by p53: a new role for the guardian of the genome. J Mol Med 2007;85:1175–86.

24. Verhaegen M, Bauer JA, Martín de la Vega C, Wang G, Wolter KG, Brenner JC, et al. A novel BH3 mimetic reveals a mitogen-activated protein kinase-dependent mechanism of melanoma cell death controlled by p53 and reactive oxygen species. Cancer Res 2006;66:11348–59.

25. Oltersdorf T, Elmore SW, Shoemaker AR, Armstrong RC, Augeri DJ, Belli BA, et al. An inhibitor of Bcl-2 family proteins induces regression of solid tumours. Nature 2005;435:677–81.

26. Friberg A, Vigil D, Zhao B, Daniels RN, Burke JP, Garcia-Barrantes PM, et al. Discovery of potent myeloid cell leukemia 1 (Mcl-1) inhibitors using fragment-based methods and structure-based design. J Med Chem 2013;56:15–30.

27. Sampietro J, Dahlberg CL, Cho US, Hinds TR, Kimelman D, Xu WQ. Crystal structure of a beta-catenin/BCL9/Tcf4 complex. Mol Cell 2006;24:293–300.

28. Kussie PH, Gorina S, Marechal V, Elenbaas B, Moreau J, Levine AJ, et al. Structure of the MDM2 oncoprotein bound to the p53 tumor suppressor transactivation domain. Science 1996;274:948–53.

29. Tovar C, Rosinski J, Filipovic Z, Higgins B, Kolinsky K, Hilton H, et al. Small-molecule MDM2 antagonists reveal aberrant p53 signaling in cancer: implications for therapy. Proc Natl Acad Sci U S A 2006;103:1888–93.

30. van Delft MF, Huang DCS. How the Bcl-2 family of proteins interact to regulate apoptosis. Cell Res 2006;16:203–13.

31. Miyashita T, Reed JC. Tumor suppressor p53 is a direct transcriptional activator of the human bax gene. Cell 1995;80:293–9.

32. Oda E, Ohki R, Murasawa H, Nemoto J, Shibue T, Yamashita T, et al. Noxa, a BH3-only member of the Bcl-2 family and candidate mediator of p53-induced apoptosis. Science 2000;288:1053–8.

33. Shibue T, Suzuki S, Okamoto H, Yoshida H, Ohba Y, Takaoka A, et al. Differential contribution of Puma and Noxa in dual regulation of p53-mediated apoptotic pathways. EMBO J 2006;25:4952–62.

34. Rew Y, Sun DQ, De Turiso FGL, Bartberger MD, Beck HP, Canon J, et al. Structure-based design of novel inhibitors of the MDM2-p53 interaction. J Med Chem 2012;55:4936–54.

35. Tovar C, Graves B, Packman K, Filipovic Z, Higgins B, Xia M, et al. MDM2 small-molecule antagonist RG7112 activates p53 signaling and regresses human tumors in preclinical cancer models. Cancer Res 2013;73:2587–97.

36. Zhao Y, Liu L, Sun W, Lu J, McEachern D, Li X, et al. Diastereomeric spirooxindoles as highly potent and efficacious MDM2 inhibitors. J Am Chem Soc 2013;135:7223–734.

37. Martins CP, Brown-Swigart L, Evan GI. Modeling the therapeutic efficacy of p53 restoration in tumors. Cell 2006;127:1323–34.

38. Xue W, Zender L, Miething C, Dickins RA, Hernando E, Krizhanovsky V, et al. Senescence and tumour clearance is triggered by p53 restoration in murine liver carcinomas. Nature 2007;445:656–60.

39. Ventura A, Kirsch DG, McLaughlin ME, Tuveson DA, Grimm J, Lintault L, et al. Restoration of p53 function leads to tumour regression in vivo. Nature 2007;445:661–5.

40. Weaver J, Downs-Kelly E, Goldblum JR, Turner S, Kulkarni S, Tubbs RR, et al. Fluorescence in situ hybridization for MDM2 gene amplification as a diagnostic tool in lipomatous neoplasms. Mod Pathol 2008;21:943–9.

41. Weaver J, Goldblum JR, Turner S, Tubbs RR, Wang WL, Lazar AJ, et al. Detection of MDM2 gene amplification or protein expression distinguishes sclerosing mesenteritis and retroperitoneal fibrosis from inflammatory well-differentiated liposarcoma. Mod Pathol 2009;22:66–70.

Cancer Research

The Journal of Cancer Research (1916–1930) | The American Journal of Cancer (1931–1940)

AACR American Association for Cancer Research

SAR405838: An Optimized Inhibitor of MDM2−p53 Interaction That Induces Complete and Durable Tumor Regression

Shaomeng Wang, Wei Sun, Yujun Zhao, et al.

Updated version	Access the most recent version of this article at: doi:10.1158/0008-5472.CAN-14-0799
Supplementary Material	Access the most recent supplemental material at: http://cancerres.aacrjournals.org/content/suppl/2014/08/21/0008-5472.CAN-14-0799.DC1

Cited articles	This article cites 39 articles, 12 of which you can access for free at: http://cancerres.aacrjournals.org/content/74/20/5855.full.html#ref-list-1
Citing articles	This article has been cited by 8 HighWire-hosted articles. Access the articles at: /content/74/20/5855.full.html#related-urls

E-mail alerts	Sign up to receive free email-alerts related to this article or journal.
Reprints and Subscriptions	To order reprints of this article or to subscribe to the journal, contact the AACR Publications Department at pubs@aacr.org.
Permissions	To request permission to re-use all or part of this article, contact the AACR Publications Department at permissions@aacr.org.